APL Materials

RESEARCH ARTICLE | JANUARY 22 2026

Growth of *a*-plane $BaTiO_3$ on *a*-plane β-Ga_2O_3 by molecular-beam epitaxy

Kathy Azizie ; Naomi A. Pieczulewski ; Nicholas A. Parker ; Jian V. Li ; Nolan S. Hendricks ;
Kyle J. Liddy ; Yorick A. Birkhölzer ; Eric A. Welp ; Luke Omodt ; Thaddeus J. Asel ; Shin Mou ;
David A. Muller ; Darrell G. Schlom

APL Mater. 14, 011110 (2026)
https://doi.org/10.1063/5.0302145

Articles You May Be Interested In

Electronic properties of ferroelectric BaTiO 3 ⁄ MgO capacitors on GaAs

Appl. Phys. Lett. (October 2004)

Oxygen vacancy induced phase and conductivity transition of epitaxial $BaTiO_{3-\delta}$ films directly grown on Ge (001) without surface passivation

J. Appl. Phys. (January 2021)

$NaNbO_3$–$BaTiO_3$–$Ba_{0.93}Ca_{0.07}TiO_3$ ceramic composites for temperature stable X8R rated dielectrics

Appl. Phys. Lett. (January 2026)

AIP Publishing

APL Materials ARTICLE pubs.aip.org/aip/apm

Growth of *a*-plane $BaTiO_3$ on *a*-plane β-Ga_2O_3 by molecular-beam epitaxy

Cite as: APL Mater. 14, 011110 (2026); doi: 10.1063/5.0302145
Submitted: 12 September 2025 • Accepted: 30 November 2025 •
Published Online: 22 January 2026

Kathy Azizie,[1] Naomi A. Pieczulewski,[1] Nicholas A. Parker,[1] Jian V. Li,[2,3] Nolan S. Hendricks,[4] Kyle J. Liddy,[4] Yorick A. Birkhölzer,[1] Eric A. Welp,[5] Luke Omodt,[5] Thaddeus J. Asel,[2] Shin Mou,[2] David A. Muller,[6,7] and Darrell G. Schlom[1,6,8,a)]

AFFILIATIONS

[1] Department of Materials Science and Engineering, Cornell University, Ithaca, New York 14853, USA
[2] Air Force Research Laboratory, Materials and Manufacturing Directorate, Wright Patterson Air Force Base, Ohio 45433, USA
[3] Core4ce, Fairborn, Ohio 45324, USA
[4] Air Force Research Laboratory, Sensors Directorate, Wright Patterson Air Force Base, Ohio 45433, USA
[5] Platform for the Accelerated Realization, Analysis, and Discovery of Interface Materials, Cornell University, Ithaca, New York 14853, USA
[6] Kavli Institute at Cornell for Nanoscale Science, Ithaca, New York 14853, USA
[7] School of Applied and Engineering Physics, Cornell University, Ithaca, New York 14853, USA
[8] Leibniz-Institut für Kristallzüchtung, Max-Born-Str. 2, 12489 Berlin, Germany

[a)] **Author to whom correspondence should be addressed:** schlom@cornell.edu

ABSTRACT

We demonstrate the epitaxial growth of single-phase (100) $BaTiO_3$ films on (100) β-Ga_2O_3 substrates at substrate temperatures ranging from 600 to 700 °C using molecular-beam epitaxy. Characterization of a 47 nm thick $BaTiO_3$ film by atomic force microscopy reveals a step-and-terrace morphology with unit-cell-high $BaTiO_3$ steps and an rms surface roughness of 0.26 nm. Scanning transmission electron microscopy (STEM) images show that in some regions the β-Ga_2O_3 substrate terminates with a (100)A plane as it transitions to $BaTiO_3$ and in other regions with a (100)B plane. The (100) $BaTiO_3$ films are fully relaxed and consist of a mixture of two types of *a*-axis domains: a_1 and a_2. The orientation relationship determined by X-ray diffraction and confirmed by STEM is (100) $BaTiO_3$ || (100) β-Ga_2O_3 and [011] $BaTiO_3$||[010] β-Ga_2O_3. Despite the average linear lattice mismatch of 3.8%, $BaTiO_3$ films with rocking curve full width at half maximum widths as narrow as 28 arc sec are achieved. From capacitance–voltage measurements on a metal–oxide–semiconductor capacitor structure with *a*-axis $BaTiO_3$ as the oxide layer and Si-doped β-Ga_2O_3 as the semiconducting layer, we extract a dielectric constant of $K_{11} = 670$ for the $BaTiO_3$ epitaxially integrated with (100) β-Ga_2O_3. We anticipate that this high-*K* epitaxial dielectric will be useful for electric-field management in β-Ga_2O_3-based device structures.

INTRODUCTION

β-Ga_2O_3 shows immense promise as a semiconductor for power electronics due to its ultra-wide bandgap (4.4–4.9 eV), large predicted breakdown field (~8 MV cm^{-1}), and mobilities that can be controlled with doping over device-relevant ranges (10^{15}–10^{19} cm^{-3}).[1–5] A common figure-of-merit of semiconductor performance in vertical power electronic devices operating at low frequency is the Baliga figure of merit (BFOM).[6–8] The BFOM can be expressed in terms of materials parameters as BFOM = $\epsilon_0 K \mu E_C^3$, where ϵ_0 is the permittivity of free space, K is the dielectric constant of the semiconductor, μ is the mobility of the charge carriers, and E_C is the electric field at which electrical breakdown of the semiconductor occurs. From the empirical dependence of E_C on the bandgap,

$E_C \approx E_g^{1.83}$,[9] this can be written as BFOM ≈ $\epsilon_0 K \mu E_g^{5.5}$. The ultra-wide bandgap of β-Ga_2O_3 results in a BFOM that compares favorably to the materials currently being used by industries for power electronics, including silicon, silicon carbide, and gallium nitride.[10,11] Furthermore, β-Ga_2O_3 has the potential to establish itself as the next-generation semiconductor material of choice as it can be grown in bulk as large single crystals for substrate production. Two leading bulk growth techniques for β-Ga_2O_3 substrates are the Czochralski (CZ)[12–14] and edge-defined film-fed growth (EFG)[15,16] methods, both of which produce large-diameter crystals from the melt by pulling a well-oriented β-Ga_2O_3 crystal along the [010] direction.

To utilize the full potential of β-Ga_2O_3 for power electronics that operate at high (>10 kV) voltages, it is essential to grow epitaxial vertical structures containing drift layers that are tens of micrometers thick with controlled donor doping in the 10^{16} cm^{-3} range.[5] For this reason, considerable progress has been made toward the development of high-quality controllably doped homoepitaxial thin-film synthesis of (010) β-Ga_2O_3 with μm h^{-1} growth rates on native substrates. Unfortunately, a common device failure that exists in thick homoepitaxial films grown on (010) β-Ga_2O_3 substrates arises from the presence of so-called nanopipes that extend along the [010] direction in bulk EFG-grown substrates.[17] Nishikawa *et al.* investigated the nature and origin of these hollow nanopipes in Sn-doped EFG-grown substrates (fabricated by Novel Crystal Technology) and noted its impact on subsequent homoepitaxial growths by hydride vapor phase epitaxy (HVPE) that influenced hillocks to form and extend into the epitaxial film from the interface.[18] These nanopipes are very detrimental for vertical structures as they act as killer defects by providing a direct leakage path through the epitaxial film into the substrate, as seen in other semiconductor materials, such as 4H–SiC—with micropipes.[19,20]

A potential solution for avoiding these nanopipes is to grow on a plane parallel to the direction of the nanopipes so that they do not propagate into the homoepitaxial layer. One candidate is the (100)-oriented β-Ga_2O_3 substrate, which is the low-energy surface of β-Ga_2O_3.[21] Although good for preventing the propagation of nanopipes, (100)-oriented β-Ga_2O_3 substrates also have challenges. For example, Schewski *et al.* demonstrated that homoepitaxial growth by metal-organic vapor phase epitaxy (MOVPE) on well-oriented (100) β-Ga_2O_3 substrates induces stacking faults in the form of twinning, resulting in a drastic reduction in the mobile carrier concentration and mobility of doped layers.[20–22] By employing substrates that are miscut by 4–6° toward $[00\bar{1}]$, these authors were able to achieve step-flow growth, twin-free films, and electron mobilities comparable with what has been achieved on (010) substrates.[22–24] When cognizant of the different growth regimes that occur as a function of miscut angle, high growth rates with high mobilities can be achieved on appropriately miscut (100) β-Ga_2O_3 substrates while minimizing both the twinning defects[25] and curtailing the influence of nanopipes that extend along the [010] direction.

Another major issue hindering the performance of vertical β-Ga_2O_3-based devices is the difficulty in terminating junctions to achieve low peak electric fields. The maximum voltage that can be applied to the devices is ideally limited only by the breakdown electric field of the β-Ga_2O_3 itself, which is predicted to be ~8 MV cm^{-1},[10] but in practice breakdown is limited to lower average fields due to stronger electric fields at junction edges. In addition to premature field-limited breakdown, edge crowding can exacerbate field-driven leakage current that similarly limits device voltage. In a Schottky junction, for example, the maximum reverse voltage is limited due to electric-field concentration at the edges of the Schottky-barrier electrode[26] or to electron tunneling from the Schottky-barrier metal into the conduction band of the β-Ga_2O_3.[27] For semiconductors that can be doped both *p*-type and *n*-type, *p*-*n* junctions can be utilized to design edge termination structures that allow devices to perform much closer to the intrinsic breakdown limits. Unfortunately, β-Ga_2O_3 can only be doped *n*-type,[28] which limits accessible devices to those that are unipolar; this complicates electric-field management.

It has been demonstrated that vertical Schottky-barrier diodes made utilizing conventional metal anodes in direct contact with β-Ga_2O_3 are limited to about 3.5 MV cm^{-1}.[27] Two techniques have overcome this limit to achieve a higher breakdown field in Schottky-barrier diodes. One approach uses a metal with a higher work function, e.g., RuO_2, IrO_2, and PtO_x, to increase the barrier height to reduce leakage current.[29–32] Another approach is to integrate a standard metal on top of a high-dielectric constant (high-*K*) barrier between the anode and β-Ga_2O_3 to lower the leakage current under an applied reverse bias.[27] Devices that utilize polycrystalline $BaTiO_3$ as the high-*K* material (with K ~ 260) in vertical Schottky barrier diodes have achieved an average breakdown field of 5.7 MV cm^{-1}, which is the highest reported to date.[27] The combination of increasing the barrier height of the anode metal and incorporating a high-*K* material has also been employed to raise the breakdown field of β-Ga_2O_3-based vertical Schottky barrier diodes.[29]

Dielectrics with higher K than the polycrystalline $BaTiO_3$ (K ~ 260)[27] or polycrystalline $BaTiO_3/SrTiO_3$ multilayers (K ~ 325)[26] that have been used with β-Ga_2O_3 for vertical Schottky barrier diodes have the potential to provide even higher breakdown fields, provided the band lineup remains favorable. At room temperature, $BaTiO_3$ is tetragonal and has considerable anisotropy in its dielectric constant. In the *a*-axis direction, single crystalline $BaTiO_3$ has $K_{11}^S = 1980$ at constant strain, which is relevant to the MHz-GHz frequency of operation; at low frequency (constant stress), it is even higher, $K_{11}^T = 4100$.[33] Along the *c*-axis direction, $K_{33}^S = 56$ at constant strain.[33] The order of magnitude increase in K that an *a*-axis oriented film of $BaTiO_3$ could bring to benefit β-Ga_2O_3-based devices compared to the polycrystalline $BaTiO_3$ films currently being used[26,27] is what motivates our study.

In this work, we tackle the challenge of integrating $BaTiO_3$ with β-Ga_2O_3 in a way that provides the direction of the highest K value in the out-of-plane direction, i.e., (100)-oriented $BaTiO_3$, on vicinal (100) β-Ga_2O_3 substrates that appear promising for vertical high-voltage β-Ga_2O_3 devices.[34] We find that (100) $BaTiO_3$ grows epitaxially on (100) β-Ga_2O_3 by molecular-beam epitaxy (MBE) over a broad range of substrate temperatures. By growing $BaTiO_3$ and Si-doped β-Ga_2O_3 on appropriately vicinal (100) β-Ga_2O_3 substrates by MBE and suboxide molecular beam epitaxy (*S*-MBE), respectively, we fabricate a metal–oxide–semiconductor capacitor (MOSCAP) and measure the epitaxial $BaTiO_3$ to have a dielectric constant in the out-of-plane direction of $K_{11} \approx 670$.

EXPERIMENTAL

Films were grown using a Veeco model GEN 10 MBE system in distilled ozone (~80% O_3 and 20% O_2 mixture). The substrate is radiatively heated by a silicon carbide filament controlled by a thermocouple and also measured by an optical pyrometer operating at a wavelength of λ = 980 nm. To ensure uniform heating, all substrates mentioned in this paper were prepared with a backside coating of ~20 nm of titanium, followed by ~200 nm of platinum. Two different substrate dimensions were utilized, 1 × 1 cm^2 (with all substrate temperatures listed measured by pyrometer) and 0.5 × 0.5 cm^2 (which required separate temperature calibration from that of a 1 × 1 cm^2 substrate). All substrate temperatures, T, listed in this work were extrapolated via optical pyrometer readings.

To grow $BaTiO_3$ films, a barium molecular beam was generated using elemental barium (Aldrich, 99.99% arc-melted into a titanium crucible) heated in a low-temperature effusion cell to working temperatures in the 520–620 °C range. The titanium molecular beam was produced by a titanium sublimation pump (Ti-Ball^{TM})[35,36] operated just below 700 W. Prior to growth, the fluxes were calibrated using a quartz crystal microbalance (QCM) in combination with interpreting reflection high-energy electron diffraction (RHEED) oscillations. Details on the calibration method used to adjust the fluxes to produce $BaTiO_3$ films and bring the Ba:Ti ratio to within 2% of being stoichiometric are provided in the supplementary material. The fluxes of barium and titanium ranged between (1–2.4) × 10^{13} atoms cm^{-2} s^{-1} (see Table I). After establishing stoichiometric fluxes on TiO_2-terminated[37] (100)-oriented $SrTiO_3$ substrates (Shinkosha), optimized $BaTiO_3$ films were then grown on well-oriented (100) Mg-doped β-Ga_2O_3 substrates grown by using the Czochralski method (boule material was provided by Synoptics and oriented, cut, and polished by CrysTec) at a background pressure of P_{O_3} = 5 × 10^{-7} Torr of distilled ozone and substrate temperatures ranging from of 600–700 °C. *In-situ* RHEED at 13 kV was used to monitor the thin-film deposition.

$BaTiO_3$ was also grown on Si-doped homoepitaxial β-Ga_2O_3 layers on treated vicinal (100) Mg-doped β-Ga_2O_3 substrates (CrysTec) miscut by 4° toward the [00$\bar{1}$] direction. This was achieved using a combination of MBE for the $BaTiO_3$[38] and suboxide MBE (*S*-MBE) for the homoepitaxial Si-doped β-Ga_2O_3 films as described elsewhere.[39,40] In brief, a Ga + Ga_2O_3 mixture containing an oxygen molar fraction of x(O) = 0.4 contained in a BeO crucible was used to generate the Ga_2O suboxide molecular beam. Similarly, SiO_2 contained in an Al_2O_3 crucible was used to produce a suboxide molecular beam of SiO. Prior to growth, the 4° miscut (100)-oriented β-Ga_2O_3 substrates were prepared following the procedure described by Schewski *et al.*[24] In particular, this substrate was sonicated in an acetone, isopropanol, and deionized water sequence (for 30 minutes each), etched in an 85% phosphoric acid aqueous solution contained in a Teflon beaker held at 140–145 °C for 15 min and then annealed for ~1 h in flowing O_2 at 900 °C. The ~500 nm thick homoepitaxial Si-doped (100)-oriented β-Ga_2O_3 film was grown at a background pressure of P_{O3} = 2.5 × 10^{-6} Torr of distilled ozone and T_{sub} = 540 °C, yielding a growth rate of ~1.0 μm h^{-1}. This was followed by a ~100 nm thick layer of stoichiometric $BaTiO_3$ grown by MBE under the conditions mentioned above with the first ~5 nm intentionally grown with 2% titanium-rich $BaTiO_3$.

X-ray diffraction (XRD), X-ray reflectivity (XRR), and pole figures were collected by a PANalytical Empyrean equipped with a hybrid incident-beam monochromator to emit Cu Kα_1 radiation on the sample. The rocking curves were measured using a triple-axis geometry with a 2-bounce Ge analyzer crystal and scintillator detector with an electron multiplier. Surface morphology and roughness were measured using an Oxford Instruments Asylum Research Cyper ES atomic force microscope (AFM) in air with tapping mode contact with Au-coated silicon AFM tips (FS-1500 AuD) operating at ~2 MHz. All AFM figures in this paper were processed using Gwyddion version 2.62, a free open-source software. Scanning transmission electron microscopy (STEM) samples were prepared using the Thermo Fisher Helios G4 UX focused ion beam with a final milling step of 5 keV. STEM measurements were taken with an aberration-corrected Thermo Fisher Spectra 300 CFEG operated at 300 keV.

The dielectric constant of $BaTiO_3$ films grown on conducting β-Ga_2O_3 buffer layers was extracted from the capacitance–voltage characteristics of a mercury-$BaTiO_3$-Si-doped Ga_2O_3 structure, which was measured by an impedance analyzer (Keysight E4990A) through a mercury probe apparatus (MDC 802B). The capacitance measurement was conducted at 10 kHz with an AC amplitude of 50 mV. The mercury probe station enabled electrical access to the $BaTiO_3$ thin film through two mercury contacts, a circular dot with an area of 0.00366 cm^2 and a concentric ring with an area of ~0.0659 cm^2. Electric field modeling was performed using a Silvaco Victory Device.

RESULTS AND DISCUSSION

The crystal structures of $BaTiO_3$ and β-Ga_2O_3 differ significantly from each other. $BaTiO_3$ is a tetragonal perovskite, which consists of corner-sharing TiO_6 oxygen coordination octahedra and barium filling the cuboctahedral interstices, while β-Ga_2O_3 is a monoclinic sesquioxide with gallium occupying both GaO_4 oxygen coordination tetrahedra as well as GaO_6 oxygen coordination octahedra. Motivated by the recent achievement of epitaxial (100)-oriented β-Ga_2O_3 films on (100) $SrTiO_3$ substrates by metal organic chemical vapor deposition (MOCVD),[41] we strive to expand this approach with the epitaxial growth of (100)-oriented $BaTiO_3$ thin films directly onto (100) β-Ga_2O_3 substrates. This employs an inverted structure relative to what has been demonstrated[41] with $BaTiO_3$ in place of $SrTiO_3$ as the perovskite-of-choice—deposited using molecular-beam epitaxy (MBE).

Figure 1 highlights both the differences and epitaxial potential between these two crystal structures. In Fig. 1(a), the unit cells of $BaTiO_3$ and β-Ga_2O_3 with the same epitaxial orientation relationship as found for the growth of β-Ga_2O_3 on (100) $SrTiO_3$,[41] i.e., (100) $BaTiO_3$ || (100) β-Ga_2O_3 and [011] $BaTiO_3$||[001] β-Ga_2O_3, are shown. The unit cell parameters listed in Fig. 1(a) are for the bulk structures at room temperature.[42,43] The substrate as drawn demonstrates a mixture of the (100)A terminated surface and the (100)B terminated surface—which according to first-principle calculations is the lowest energy surface of β-Ga_2O_3.[21] An isometric, side-view, and top-view of the observed orientation relationship is shown in Figs. 1(a)–1(c). Here, the terminated β-Ga_2O_3 (100)A and (100)B surfaces are highlighted and the outline of the surface unit cell of (100) $BaTiO_3$, the surface unit cell of (100) β-Ga_2O_3 and the surface unit cell of the near-coincident-site lattice (NCSL)[44] of this $\sigma_{BaTiO_3}2\ :\ \sigma_{Ga_2O_3}2$ interface are shown. In Fig. 1(c), the unit cell of the NCSL at the interface between (100) $BaTiO_3$ and (100) β-Ga_2O_3 is outlined so that its makeup with respect to the (100) $BaTiO_3$ and (100) β-Ga_2O_3 unit cells is evident. The lattice match along the perpendicular axes of the NCSL unit cell are seen to be +2.1% along one axis ($[0\bar{1}1]$ $BaTiO_3$ ∥ [001] β-Ga_2O_3) of the NCSL and +7.0% along the perpendicular axis ([011] $BaTiO_3$∥[010] β-Ga_2O_3) of the NCSL. This areal lattice match corresponds to an average linear lattice match of +3.8%. At room temperature, $BaTiO_3$ has a tetragonal distortion from being cubic, with the c axis about 1% longer than the a axis. To best satisfy the lattice match to (100) β-Ga_2O_3, where both in-plane directions are larger than the axes of $BaTiO_3$, the longer axis of $BaTiO_3$ (the c axis) lies in the (100) plane of the β-Ga_2O_3 substrate and the shortest axis of $BaTiO_3$ (the a axis) lies in the out-of-plane direction, as depicted in Fig. 1. As we describe in the following, this epitaxial relationship is what we observe.

Initially, a series of $BaTiO_3$ films were grown under the conditions listed in Table I (samples A–F), on well-oriented Mg-doped (100) β-Ga_2O_3 substrates (with offcuts <1°) to explore the growth parameters under which epitaxial $BaTiO_3$ can be achieved by MBE. We explored a substrate temperature range of 600–700 °C with a targeted thicknesses of ~40 nm. The resulting films grown over this temperature range are epitaxial as manifested in the *in-situ* RHEED patterns and *ex-situ* XRD measurements made after growth. Figure 2 shows both the XRD scans and RHEED patterns of these films.

The dashed lines in Figs. 2(a) and 2(b) show the calculated positions of where the 00ℓ and $h00$ family of (relaxed) tetragonal $BaTiO_3$ peaks would occur. The differences between the two orientations are most notable at higher-order peaks. For instance, c-plane (relaxed) $BaTiO_3$ would have an identifiable 003 peak at $2\theta \approx 69.8^\circ$ whereas a-plane (relaxed) $BaTiO_3$ would show a signature 300 peak at $2\theta \approx 70.6^\circ$. In our experimental data, we see the presence of only the $h00$ family of $BaTiO_3$ peaks in the θ-2θ X-ray diffraction spectra, which are consistent with the films being single-phase (100)-oriented tetragonal $BaTiO_3$, i.e., a-plane $BaTiO_3$. Figure 2(b) shows a close-up of the 100 $BaTiO_3$ peak of the $BaTiO_3$ films samples A-F.

The 300 and 900 peaks of β-Ga_2O_3 are forbidden, making it easy to discern the 100 and 300 $BaTiO_3$ peaks, respectively. In contrast, the 200 $BaTiO_3$ peak overlaps with the 600 peak of the β-Ga_2O_3 substrate. To combat the peak splitting observed in the pole scans about the 100 $BaTiO_3$ peak (Fig. S1), we align the a axis of the film to be parallel to the ϕ-axis of the diffractometer and the miscut direction of the substrate to be perpendicular to the projection of the incident X-ray beam on the substrate. Such alignment makes it so that clear Laue oscillations are visible around the 100 $BaTiO_3$ peak in many of the films.[45] These same films show clear Kiessig fringes in XRR.[46] These fringes and oscillations are indicative of a smooth $BaTiO_3$ film with uniform thickness and were used to accurately quantify the $BaTiO_3$ film thicknesses given in Table I.

The films in Fig. 2(b) display some variability in the position of the 100 $BaTiO_3$ peak from that of a relaxed a-axis $BaTiO_3$ peak, as indicated by the dashed line. As a result, the out-of-plane lattice

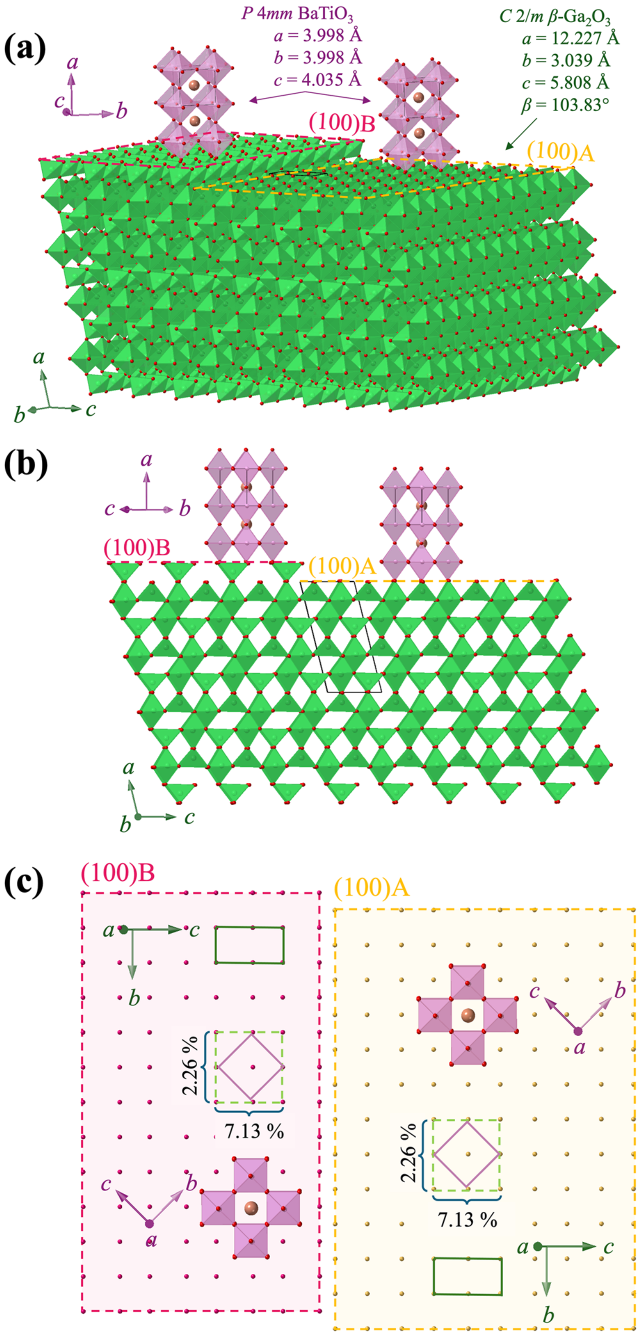

FIG. 1. Schematic of the epitaxial orientation relationship between $BaTiO_3$ as the film to β-Ga_2O_3 as the underlying substrate with its dominant terminated planes, (100)A and (100)B, as (a) an isometric, (b) side-view (along the [111] and [010] axes of $BaTiO_3$ and Ga_2O_3 respectively), and (c) a top-view (along the [100] zone axis of both $BaTiO_3$ and β-Ga_2O_3) with only the Ga_2O_3 oxygens present. (c) In addition, outlines of the unit cell of a-plane $BaTiO_3$ (purple), a-plane Ga_2O_3 (green), and of the near coincidence site lattice (NCSL) of the $\sigma_{BaTiO_3}2\ :\ \sigma_{Ga_2O_3}2$ interface between (100) $BaTiO_3$ and (100) β-Ga_2O_3 (dashed green). This lattice mismatch between the NCSL with the underlying β-Ga_2O_3 are given as percentages.

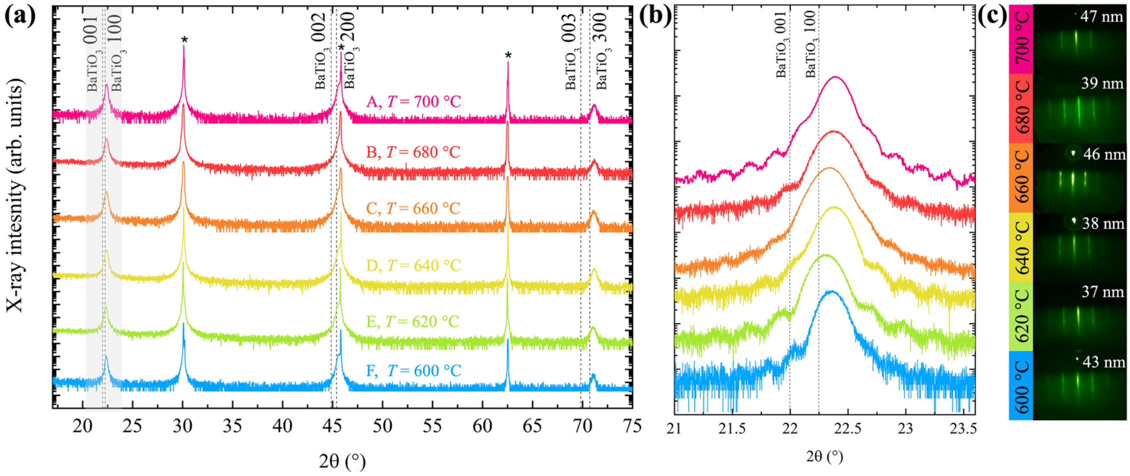

FIG. 2. (a) θ-2θ X-ray diffraction scans of $BaTiO_3$ films grown on Mg-doped (100)-oriented β-Ga_2O_3 substrates grown with a T_{sub} value ranging from 600 to 700 °C with (b) a finer scan around the 100 $BaTiO_3$ peak showing the presence of Laue oscillations. (c) The smoothness and epitaxial growth of the films is further supported by RHEED patterns taken along the <011> azimuth of the $BaTiO_3$ at the end of the growth of each film with their respective thicknesses (white text) as confirmed by X-ray reflectivity analysis. The h00 peaks of the β-Ga_2O_3 substrate, where h is an even integer, are marked by the asterisks (*).

constant, listed in Table I, reflects this spread when compared to the expected out-of-plane lattice spacing of a relaxed stoichiometric a-axis $BaTiO_3$ film, 3.998 Å.[43] A likely reason for this deviation in the peak positions and out-of-plane lattice constants is the barium to titanium ratio being slightly off-stoichiometry from 1:1. The lattice constant of $BaTiO_3$ films have been shown to vary with off-stoichiometry.[47–49] This implies that the films with a peak position closest to the dashed line are the closest to stoichiometric $BaTiO_3$.

The epitaxy was monitored throughout the growth by *in-situ* RHEED. Figure 2(c) shows RHEED patterns taken at the end of growth for the corresponding films described in Table I. The RHEED patterns in Fig. 2(c) are taken with the electron beam incident along the [011] $BaTiO_3$ azimuth. The films in Fig. 2(c) show intense and clear streaks without any presence of half-order streaks, which if they were present would be indicative of barium-rich $BaTiO_3$.[50] The use of these indicators suggests that during growth, the films are slightly titanium-rich with smooth surfaces. The extent of this near-stoichiometric, epitaxial growth window was mapped-out over a range of substrate temperatures shown in Fig. 2(c). Growths below a substrate temperature of 600 °C were observed by RHEED to be polycrystalline, as shown in Fig. S2. The combination of the X-ray diffraction and RHEED results show that these films are epitaxial a-plane $BaTiO_3$ with no impurity phases present. In addition, a ϕ scan of sample C (Fig. S5) corroborates the epitaxial alignment seen in RHEED, in agreement with Fig. 1.

The smoothness of these films is corroborated by AFM imaging of the surface of the as-grown films. AFM imaging of sample C, which has the lowest substrate miscut (~0.06°), is shown in Figs. 3(a) and 3(b). Figure 3(a) shows a step-and-terrace surface morphology that spans over a relatively large scan size of $10 \times 10\ \mu m^2$ area with an

TABLE I. Characteristics of $BaTiO_3$ samples grown at $P_{O_3} = 5 \times 10^{-7}$ Torr (~80% distilled ozone).

Name	T_{pyro} (°C)	$BaTiO_3$ film thickness (nm)	$BaTiO_3$ growth rate (nm h^{-1})	Ba flux (atoms cm^{-2})	Ti flux (atoms cm^{-2})	Film rocking FWHM (°)[a]	Substrate rocking FWHM (°)[a]	Out-of-plane spacing (Å)	rms roughness (nm)[a]	Miscut angle (°)
Sample A	700	47	14.4	6.2×10^{12}	6.2×10^{12}	0.013	0.006	3.97	0.23	0.21
Sample B	680	39	15.7	6.8×10^{12}	6.8×10^{12}	0.03	0.03	3.97	0.24	1.30
Sample C	660	46	58.8	2.5×10^{13}	2.5×10^{13}	0.008	0.009	3.97	0.26	0.01
Sample D	640	38	17.1	7.3×10^{12}	7.3×10^{12}	0.04	0.01	3.97	0.12	0.13
Sample E	620	37	15.7	6.8×10^{12}	6.8×10^{12}	0.05	0.04	3.98	0.094	0.87
Sample F	600	43	14.4	6.2×10^{12}	6.2×10^{12}	0.015	0.02	3.98	0.29	0.35
Sample G	700	109	26.4	1.2×10^{13}	1.2×10^{13}	0.77	0.005	4.00	4.9	4.00

[a] See the supplementary material for rocking curves (Fig. S6) and AFM (Fig. S7) scans from which these values were extracted.

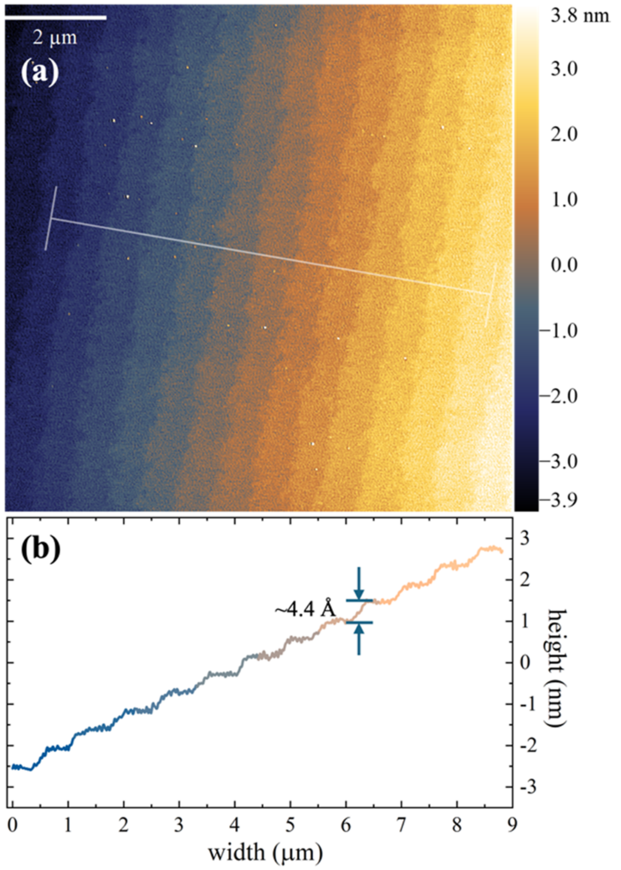

FIG. 3. Atomic force microscopy scans of sample C, a $BaTiO_3$ film grown on an Mg-doped (100) oriented β-Ga_2O_3 substrate at a substrate temperature of 660 °C. (a) 10×10 μm^2 scan illustrating the step-and-terrace morphology of the sample with an rms roughness of 262 pm. Panel (b) depicts a line scan of the white-lined path mapped across the 10×10 μm^2 scan (a), showcasing the step-like surface of the $BaTiO_3$ film with an average step-height of ~4.4 Å.

rms roughness of 0.26 nm. Generating a line scan across these steps, shown in Fig. 3(b), reveals steps with an average height of ~4.4 Å; which corresponds nicely to the height of a unit cell of $BaTiO_3$. Notably, AFM on all of the films in Table I revealed rms roughnesses <0.3 nm.

STEM characterization was further performed on the $BaTiO_3$ film grown on a well-oriented (100) Mg-doped β-Ga_2O_3 substrate (sample C). To understand the interface structure between $BaTiO_3$ and β-Ga_2O_3, integrated differential phase contrast (iDPC) imaging was performed to allow visualization of light elements, such as oxygen. Figure 4(a) shows the iDPC image of the atomically sharp interface between the $BaTiO_3$ film and β-Ga_2O_3 substrate. Here, we see that the β-Ga_2O_3 substrate surface possesses steps exposing both the (100)A and (100)B planes[21] as the surface termination layer. An edge dislocation is also often observed at the step edge between these differently terminated planes. In Fig. 4(b), a larger field-of-view high-angle annular dark-field scanning transmission electron microscopy (HAADF-STEM) image of the $BaTiO_3$ and β-Ga_2O_3 substrate interface is shown. While the clean, sharp interface is consistently preserved, the $BaTiO_3$ film is made up of many small domains (<10 nm in size). The domains and edge dislocations within the domains likely enable the $BaTiO_3$ to relax the strain from substrate step edges and 3.8% lattice mismatch. The edge dislocations were identified by masking in-plane diffraction peaks to visualize lattice planes (see Fig. S3 in the supplementary material).

A fast Fourier transform (FFT) of the entire region shown in the inset of Fig. 4(b) that confirms that the domains of $BaTiO_3$ are fully relaxed from the β-Ga_2O_3 substrate, with the in-plane d-spacing measured to be between the expected d-spacing for a-axis and c-axis $BaTiO_3$. The relaxation is most apparent when comparing the $h2\bar{2}$ family of $BaTiO_3$ diffraction peaks (magenta) with respect to the $h1\bar{2}$ family of β-Ga_2O_3 diffraction peaks (green), where the $BaTiO_3$ crystal displays smaller in-plane lattice parameters. This in-plane relaxation is also seen in the reciprocal space mappings of samples C and G (Fig. S4).

Figures 4(c) and 4(d) show angular dark field (ADF) images with different magnifications that scope the entire $BaTiO_3$ film spanning from the β-Ga_2O_3 substrate up to the sample surface. In both figures, threading dislocations can be seen originating at the substrate interface and annihilate after ~10 nm from the interface [dashed line in Fig. 4(d)] into highly ordered large domains (>20 nm in size).

To demonstrate the difference of these $BaTiO_3$ domains, Fig. 4(e) overlaps the FFT of two neighboring regions of $BaTiO_3$ boxed as red and cyan in Fig. 4(c). The boxed regions in orange and gray highlight the third-order diffraction peaks, where subtle lattice-parameter-differences are more exasperated. In the gray boxed region, the $03\bar{3}$ $BaTiO_3$ diffraction peak shows only in-plane lattice parameter shifts, with only horizontal shifts seen between the red and cyan whereas in the orange boxed-region, the $\bar{3}00$ $BaTiO_3$ diffraction peaks are overlapping, showing no out-of-plane lattice parameter differences. This shows that the in-plane lattice constants differ, while the out-of-plane lattice constant are similar, which indicates that there is a mixture of a_1 and a_2 domains. That both a_1 and a_2 domains are present is also consistent with the ϕ scan of this sample shown in Fig. S5.

After confirming with STEM that epitaxial a-axis oriented $BaTiO_3$ thin films—the orientation with the highest out-of-plane dielectric constant, K_{11}—can be achieved directly onto well-oriented (100) β-Ga_2O_3 substrates, we next determine the dielectric constant of this crystalline $BaTiO_3$ layer. To measure the dielectric constant, we create a metal–oxide–semiconductor capacitor (MOSCAP) structure, with $BaTiO_3$ as the oxide layer and Si-doped β-Ga_2O_3 as the semiconducting layer. To achieve this structure on (100) Ga_2O_3 substrates while avoiding the reduced mobilities and electron concentrations as seen by Fiedler *et al.* in homoepitaxial growths of Si-doped β-Ga_2O_3 by MOCVD on well-oriented (100) Ga_2O_3 substrates,[23] we utilized a 4° vicinal (100) Mg-doped β-Ga_2O_3 substrate with an offcut toward $[00\bar{1}]$, which has been shown to work by the same authors. Si-doped β-Ga_2O_3 was grown using the S-MBE technique outlined by Azizie *et al.*[40] with a growth rate of ~1.04 $\mu m\ h^{-1}$ to a thickness of ~500 nm with a targeted doping concentration of 1×10^{20} cm^{-3}. The subsequent layer, $BaTiO_3$, was grown on top

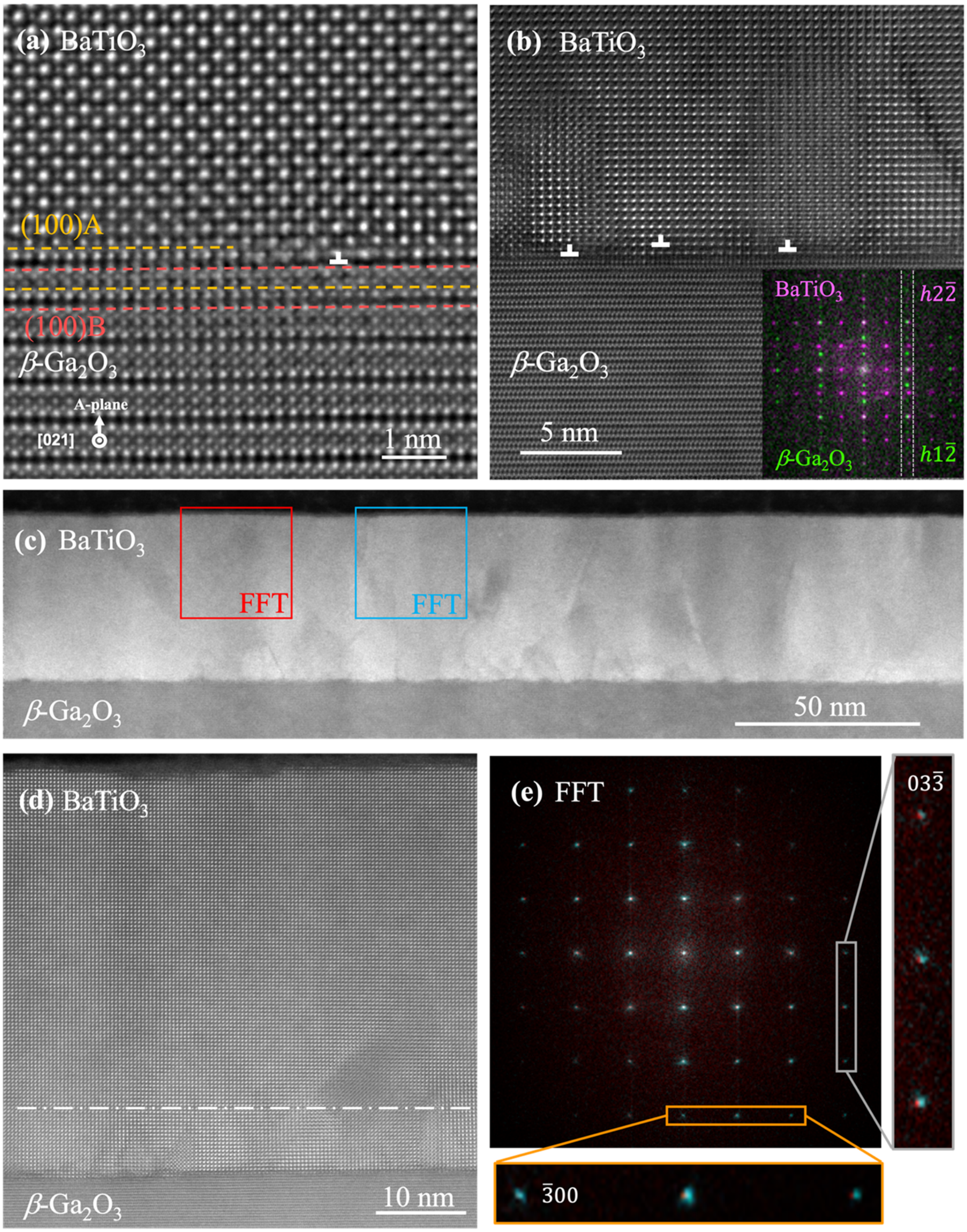

FIG. 4. Series of cross-sectional images of sample C, $BaTiO_3$ film grown epitaxially on a well-oriented Mg-doped *a*-plane β-Ga_2O_3 substrate. (a) iDPC image of the sharp interface between the $BaTiO_3$ film and regions where the β-Ga_2O_3 substrate is terminated by (100)A and (100)B planes are seen, as delineated by the dashed lines (yellow and red, respectively). Panel (b) is a zoomed-in view of a different region that highlights edge dislocations at the interface with an overlaid fast Fourier transform (FFT) of the entire region inset that shows that the $BaTiO_3$ (purple) is fully relaxed from β-Ga_2O_3 (green). (c) The lowest magnification image depicts the entire crystal structure of the $BaTiO_3$ film, including a few screw dislocations marked with arrows that arise from the substrate/film interface and terminate about ∼10 nm into the film. Panel (d) shows the defects present at the substrate interface—that terminates at the dashed line ∼10 nm from the substrate interface—when compared to rest of the grown $BaTiO_3$ film, which shows a highly ordered structure until the surface. Panel (e) shows the resulting overlapping FFT of the $BaTiO_3$ film near the surface from different boxed regions shown in panel (c). Notably, only subtle horizontal shifts are visible in the FFT overlap with no vertical shifts (better seen in blown ups of regions boxed in gray and orange); this supports the existence of a_1 and a_2 domains.

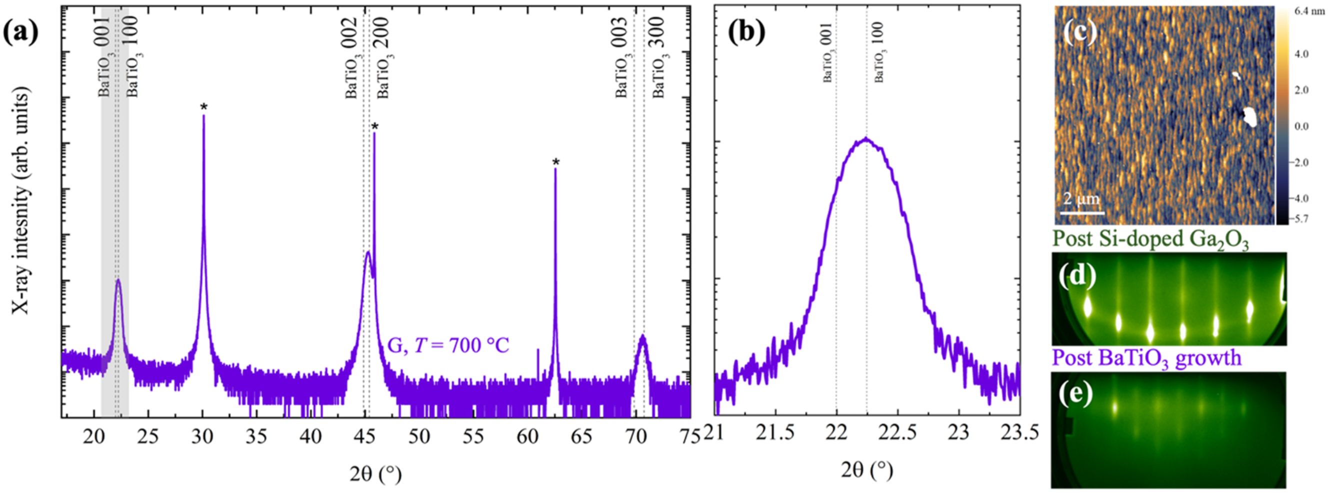

FIG. 5. Structural characterization of sample G: 109 nm thick (100) $BaTiO_3$ on ∼500 nm thick Si-doped (100) β-Ga_2O_3 (with a targeted doping concentration of 1×10^{20} cm^{-3}) onto a vicinal 4° (100)-oriented Mg-doped β-Ga_2O_3 substrate with an offcut toward [00$\bar{1}$]. (a) θ-2θ X-ray diffraction scan and (b) finer scan around the 100 $BaTiO_3$ diffraction peak with both the h00 and 00ℓ family of $BaTiO_3$ peaks marked with the dashed lines, while all substrate peaks are marked by asterisks (*). *In-situ* RHEED patterns along the [001] azimuth of the (c) bare substrate prior to growth and (d) $BaTiO_3$ film after growth. (e) AFM of a 10×10 μm^2 area with a rms roughness of 4.9 nm.

without breaking vacuum. The first ∼5 nm of the $BaTiO_3$ layer was intentionally grown 2% titanium rich from stoichiometric to improve nucleation and the remaining ∼100 nm of $BaTiO_3$ was grown with a 1:1 barium-to-titanium ratio.

Figure 5 shows the resulting structural characterization of this MOS stack by RHEED, XRD, and AFM. The XRD scan, Fig. 5(a), clearly illustrates the presence of only the β-Ga_2O_3 substrate and the h00 family of $BaTiO_3$ film peaks over a long-range scan, with Fig. 5(b) showing a close-up of the 100 $BaTiO_3$ film peak. The position of the peak in Fig. 5(b) is again more consistent with the film being a-axis oriented $BaTiO_3$ rather than c-axis oriented $BaTiO_3$, as indicated by the dashed lines. The out-of-plane lattice parameter of the $BaTiO_3$ thin film from these scans, calculated by the Nelson-Riley function,[51] is 4.00 ± 0.007 Å. This value is within experimental error of the a-axis lattice constant of $BaTiO_3$. *In-situ* RHEED of the bare substrate prior to growth, Fig. 5(c), and post growth, Fig. 5(d), reveal epitaxial growth of $BaTiO_3$ on the 4° vicinal (100) β-Ga_2O_3 substrate. The RHEED pattern exhibits a characteristic transition from sharp, well-defined streaks of the bare substrate to weaker and more diffuse transmission diffraction pattern indicative of less perfect crystalline order and a rougher film. This observation is corroborated by a post-growth AFM scan, Fig. 5(e), with an rms roughness of 4.9 nm.

Figure 6(a) shows the mercury-probed capacitance–voltage characteristics (diamond symbols) of the epitaxial $BaTiO_3$ thin film grown on top of the Si-doped β-Ga_2O_3 layer (sample G). If we treat the maximum capacitance shown in Fig. 6(a) as being solely contributed by the $BaTiO_3$ thin film contacted by the mercury dot, its dielectric constant is roughly estimated to be 417. A more accurate description of the capacitance–voltage curve requires an equivalent circuit model that includes four capacitances connected in series: two contributed by $BaTiO_3$ and β-Ga_2O_3, respectively, in the area contacted by the mercury dot, and another two contributed similarly in the area contacted by the mercury ring. The $BaTiO_3$-associated capacitances are independent of bias whereas the β-Ga_2O_3 semiconductor-associated capacitors are bias-dependent. A dielectric constant of K_{11} = 670 was extracted for the a-axis oriented $BaTiO_3$ thin film by fitting the experimental data to the four-capacitance model, as shown in Fig. 6(a) indicated by the solid purple line. This dielectric constant is not as high as that obtained on monodomain, high-quality a-axis $BaTiO_3$ single crystals (K_{11}^S = 1980);[33] this could be due to the lower structural quality of our film. Nonetheless, the dielectric constant of our $BaTiO_3$ film greatly exceeds that of all prior $BaTiO_3$ films on β-Ga_2O_3 and motivates its use for electric field management in β-Ga_2O_3-based devices.

For instance, Fig. 6(b) showcases the electric field modeling to estimate the effect of the dielectric constant (K) of the $BaTiO_3$ layer in a simulated device with a 55 nm thick layer of $BaTiO_3$ on a β-Ga_2O_3 layer with (N_D−N_A) of 2×10^{16} cm^{-3} at 1200 V. Assuming that the $BaTiO_3$ permittivity is isotropic and that there is no electric-field dependence on the permittivity, we see in Fig. 6(c) that with an average electric field under the anode of 2.9 MV cm^{-1}, the modeled peak electric field in the β-Ga_2O_3 is decreased from 9.2 to 7.4 MV cm^{-1}, when comparing K from the 260 reported for polycrystalline $BaTiO_3$/β-Ga_2O_3[27] to the 670 that we report for epitaxial $BaTiO_3$/β-Ga_2O_3 in this work. By being able to epitaxially integrate a high K $BaTiO_3$ layer, we can achieve up to a 20% decrease in the peak electric field. The ability to integrate a layer with such high K is just one advantage of the (100) β-Ga_2O_3 orientation among several others.

Vicinal (100) β-Ga_2O_3 substrates appear to have multiple advantages relevant to device technology. First, the (100) β-Ga_2O_3 surface has the lowest surface energy,[21] enabling step-flow growth to

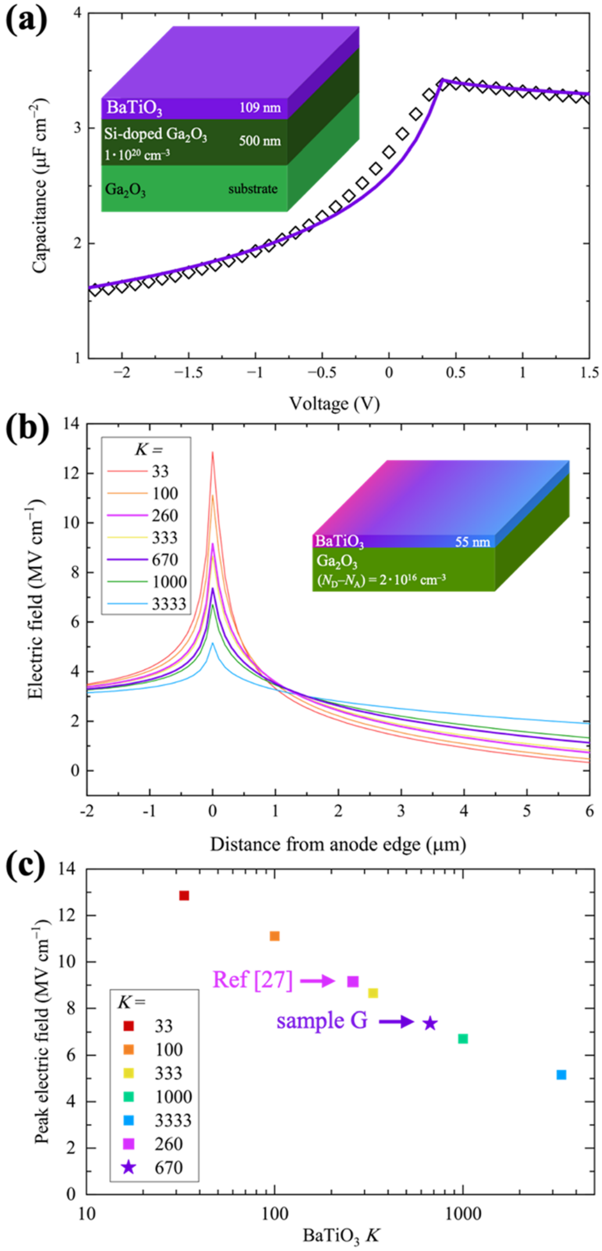

FIG. 6. Panel (a) shows the growth structure of sample G, a BaTiO$_3$-on-conductive-Ga$_2$O$_3$ MOS capacitor, measured by using an impedance analyzer through a mercury probe to obtain the capacitance–voltage characteristics. A dielectric constant (K) of 670 was extracted for the BaTiO$_3$ film by fitting the experiment data (diamond symbols) to an equivalent-circuit model (purple-line) accounting for relevant capacitive contributions of the BaTiO$_3$ thin film and the underlying β-Ga$_2$O$_3$ buffer at the probing locations. Panel (b) compiles the calculated electric fields for select BaTiO$_3$ dielectric constants to the structure embedded—a thick 55 nm layer of BaTiO$_3$ onto a β-Ga$_2$O$_3$ layer with (N_D-N_A) of ∼2 × 10^{16} cm^{-3}—including experimental results from Ref. 27 with a K = 260 (violet) and sample G—from this work (purple) with a K = 670. Panel (c) plots the peak electric field of each K from panel (b), with Ref. 27 having a peak electric field of 9.2 MV cm^{-1} and sample G—7.4 MV cm^{-1}.

produce thick films with smooth surfaces. The low surface energy of (100) β-Ga$_2$O$_3$ also enables heterostructures involving commensurate β-(Al,Ga)$_2$O$_3$ layers to be grown (without cracks and relaxation of the commensurate strain) with either higher aluminum contents for the same thickness or as thicker films for the same aluminum content.[21] Furthermore, the conduction band offset is the greatest between commensurate β-(Al,Ga)$_2$O$_3$ and β-Ga$_2$O$_3$ layers grown on (100) β-Ga$_2$O$_3$.[52] The aforementioned properties are all advantageous for bandgap engineering. This orientation also has high demonstrated mobility[53] and likely overcomes the nanopipe killer defect problem.[18] Finally, as demonstrated by this work, growth on vicinal (100) β-Ga$_2$O$_3$ substrates enables the epitaxial integration of BaTiO$_3$ films in the orientation with the highest dielectric constant, a win for electric field management in β-Ga$_2$O$_3$-based power electronic devices.

CONCLUSION

We were able to successfully grow epitaxial and atomically smooth (100) BaTiO$_3$ films onto well-oriented (100) β-Ga$_2$O$_3$ substrates by MBE. Optimal growth conditions for BaTiO$_3$ were informed by both *in-situ* and *ex-situ* analysis techniques including RHEED, XRD, XRR, AFM, and STEM. After establishing epitaxial BaTiO$_3$ growths on well-oriented (100) β-Ga$_2$O$_3$ substrates, we then integrated this perovskite onto a 4° vicinal Mg-doped (100) β-Ga$_2$O$_3$ substrate to produce a MOSCAP, enabling the dielectric constant of the epitaxial a-axis BaTiO$_3$ to be determined. The result, K_{11} = 670, is more than twice as high as all prior dielectrics that have been integrated with β-Ga$_2$O$_3$.[26,27] In addition to the potential of epitaxial a-axis oriented BaTiO$_3$ films on (100) β-Ga$_2$O$_3$ substrates to overcome the limited breakdown field that β-Ga$_2$O$_3$ experiences in vertical Schottky-barrier diode devices, it also provides an avenue for the integration of other perovskites onto monoclinic (100) β-Ga$_2$O$_3$. BaTiO$_3$ is the first perovskite to ever be epitaxially integrated with β-Ga$_2$O$_3$ and this demonstration opens the door for the integration of other perovskite materials with a potpourri of exciting functional properties (ferromagnetism, multiferroics, high spin polarization, superconductivity, etc.) to be exploited in β-Ga$_2$O$_3$-based electronics.

SUPPLEMENTARY MATERIAL

See the supplementary material for additional characterization of the samples in this paper including reciprocal space mappings (RSM), rocking curves, atomic force microscopy (AFM), and pole figures.

ACKNOWLEDGMENTS

We thank Bennett Cromer, Hari Nair, and Huili (Grace) Xing for fruitful discussions. K.A., N.A. Pieczulewski, D.A.M., and D.G.S. acknowledge support from the AFOSR/AFRL ACCESS Center of Excellence under Award No. FA9550-18-1-0529. N.A. Pieczulewski acknowledges support from the National Science Foundation (NSF) Graduate Research Fellowship Program (GRFP) (Grant No. DGE21139899). J.V.L., T.J.A., and S.M. acknowledge financial support from AFOSR (Lab Task 23RXCOR017). Y.A.B.

acknowledges support from SUPREME, one of the seven centers in JUMP 2.0, a Semiconductor Research Corporation (SRC) program sponsored by DARPA. N.A. Parker and E.A.W. acknowledge support from the NSF [Platform for the Accelerated Realization, Analysis and Discovery of Interface Materials (PARADIM)] under Cooperative Agreement No. DMR-2039380. This work made use of the Cornell Center for Materials Research (CCMR) Shared Facilities, which are supported through the NSF MRSEC Program (Grant No. DMR-1719875). Substrate preparation was performed, in part, at the Cornell NanoScale Facility, a member of the National Nanotechnology Coordinated Infrastructure (NNCI), which is supported by the NSF (Grant No. NNCI-2025233).

AUTHOR DECLARATIONS

Conflict of Interest

The authors K.A. and D.G.S. have been granted U.S. Patent No. 11 462 402 (October 4, 2022) with the title "Suboxide Molecular-Beam Epitaxy and Related Structures."

Author Contributions

Kathy Azizie: Conceptualization (equal); Data curation (equal); Formal analysis (equal); Investigation (equal); Validation (equal); Visualization (equal); Writing – original draft (equal); Writing – review & editing (equal). **Naomi A. Pieczulewski**: Data curation (supporting); Formal analysis (supporting); Investigation (supporting); Validation (equal); Visualization (equal); Writing – original draft (supporting); Writing – review & editing (equal). **Nicholas A. Parker**: Data curation (supporting); Investigation (supporting); Validation (supporting); Visualization (supporting); Writing – review & editing (supporting). **Jian V. Li**: Data curation (supporting); Formal analysis (supporting); Investigation (supporting); Validation (supporting); Visualization (supporting); Writing – original draft (supporting); Writing – review & editing (supporting). **Nolan S. Hendricks**: Data curation (supporting); Investigation (supporting); Visualization (equal); Writing – original draft (supporting); Writing – review & editing (supporting). **Kyle J. Liddy**: Data curation (supporting); Formal analysis (supporting); Visualization (supporting). **Yorick A. Birkhölzer**: Data curation (supporting); Formal analysis (supporting); Validation (supporting); Visualization (supporting); Writing – review & editing (supporting). **Eric A. Welp**: Data curation (supporting); Investigation (supporting); Validation (supporting); Visualization (supporting); Writing – review & editing (supporting). **Luke Omodt**: Data curation (supporting); Investigation (supporting). **Thaddeus J. Asel**: Data curation (supporting); Formal analysis (supporting); Funding acquisition (supporting); Resources (supporting); Validation (supporting); Writing – review & editing (supporting). **Shin Mou**: Funding acquisition (supporting); Project administration (supporting); Resources (supporting); Visualization (supporting). **David A. Muller**: Data curation (equal); Investigation (supporting); Methodology (supporting); Project administration (equal); Resources (equal); Validation (equal). **Darrell G. Schlom**: Conceptualization (lead); Formal analysis (equal); Funding acquisition (lead); Investigation (equal); Project administration (lead); Supervision (lead); Visualization (equal); Writing – original draft (equal); Writing – review & editing (equal).

DATA AVAILABILITY

The data support the findings of this study are available within the paper. Additional data related to the growth and structural characterization are available at https://doi.org/10.34863/ds11-av32. Any additional data connected to the study are available from the corresponding author upon reasonable request.

REFERENCES

[1] H. H. Tippins, "Optical absorption and photoconductivity in the band edge of β-Ga_2O_3," Phys. Rev. **140**, A316–A319 (1965).

[2] M. Higashiwaki, H. Murakami, Y. Kumagai, and A. Kuramata, "Current status of β-Ga_2O_3 power devices," Jpn. J. Appl. Phys. **55**, 1202A1 (2016).

[3] M. Higashiwaki and G. H. Jessen, "Guest editorial: The dawn of gallium oxide microelectronics," Appl. Phys. Lett. **112**, 060401 (2018).

[4] Z. Galazka, "β-Ga_2O_3 for wide-bandgap electronics and optoelectronics," Semicond. Sci. Technol. **33**, 113001 (2018).

[5] A. J. Green, J. Speck, G. Xing, P. Moens, F. Allerstam, K. Gumaelius, T. Neyer, A. Arias-Purdue, V. Mehrotra, A. Kuramata, K. Sasaki, S. Watanabe, K. Koshi, J. Blevins, O. Bierwagen, S. Krishnamoorthy, K. Leedy, A. R. Arehart, A. T. Neal, S. Mou, S. A. Ringel, A. Kumar, A. Sharma, K. Ghosh, U. Singisetti, W. Li, K. Chabak, K. Liddy, A. Islam, S. Rajan, S. Graham, S. Choi, Z. Cheng, and M. Higashiwaki, "β-gallium oxide power electronics," APL Mater. **10**, 029201 (2022).

[6] B. J. Baliga, "Semiconductors for high-voltage, vertical channel field-effect transistors," J. Appl. Phys. **53**, 1759–1764 (1982).

[7] B. J. Baliga, "Power semiconductor device figure of merit for high-frequency applications," IEEE Electron Device Lett. **10**(10), 455–457 (1989).

[8] B. J. Baliga, *Fundamentals of Power Semiconductor Devices*, 2nd ed. (Springer, 2019) pp. 14–16.

[9] O. Slobodyan, J. Flicker, J. Dickerson, J. Shoemaker, A. Binder, T. Smith, S. Goodnick, R. Kaplar, and M. Hollis, "Analysis of the dependence of critical electric field on semiconductor bandgap," J. Mater. Res. **37**, 849–865 (2022).

[10] M. Higashiwaki, K. Sasaki, A. Kuramata, T. Masui, and S. Yamakoshi, "Gallium oxide (Ga_2O_3) metal-semiconductor field-effect transistors on single-crystal β-Ga_2O_3 (010) substrates," Appl. Phys. Lett. **100**, 013504 (2012).

[11] J. Y. Tsao, S. Chowdhury, M. A. Hollis, D. Jena, N. M. Johnson, K. A. Jones, R. J. Kaplar, S. Rajan, C. G. Van de Walle, E. Bellotti, C. L. Chua, R. Collazo, M. E. Coltrin, J. A. Cooper, K. R. Evans, S. Graham, T. A. Grotjohn, E. R. Heller, M. Higashiwaki, M. S. Islam, P. W. Juodawlkis, M. A. Khan, A. D. Koehler, J. H. Leach, U. K. Mishra, R. J. Nemanich, R. C. N. Pilawa-Podgurski, J. B. Shealy, Z. Sitar, M. J. Tadjer, A. F. Witulski, M. Wraback, and J. A. Simmons, "Ultrawide-bandgap semiconductors: Research opportunities and challenges," Adv. Electron. Mater. **4**(1), 1600501 (2018).

[12] Y. Tomm, P. Reiche, D. Klimm, and T. Fukuda, "Czochralski grown Ga_2O_3 crystals," J. Cryst. Growth **220**, 510–514 (2000).

[13] Z. Galazka, R. Uecker, K. Irmscher, M. Albrecht, D. Klimm, M. Pietsch, M. Brützam, R. Bertram, S. Ganschow, and R. Fornari, "Czochralski growth and characterization of β-Ga_2O_3 single crystals," Cryst. Res. Technol. **45**(12), 1229–1236 (2010).

[14] Z. Galazka, K. Irmscher, R. Uecker, R. Bertram, M. Pietsch, A. Kwasniewski, M. Naumann, T. Schulz, R. Schewski, D. Klimm, and M. Bickermann, "On the bulk β-Ga_2O_3 single crystals grown by the Czochralski method," J. Cryst. Growth **404**, 184–191 (2014).

[15] H. Aida, K. Nishiguchi, H. Takeda, N. Aota, K. Sunakawa, and Y. Yaguchi, "Growth of β-Ga_2O_3 single crystals by edge-defined, film fed growth method," Jpn. J. Appl. Phys. **47**, 8506–8509 (2008).

[16] A. Kuramata, K. Koshi, S. Watanabe, Y. Yamaoka, T. Masui, and S. Yamakoshi, "High-quality β-Ga_2O_3 single crystals grown by edge-defined film-fed growth," Jpn. J. Appl. Phys. **55**, 1202A2 (2016).

[17] K. Nakai, T. Nagai, K. Noami, and T. Futagi, "Characterization of defects in β-Ga_2O_3 single crystals," Jpn. J. Appl. Phys. **54**, 051103 (2015).

[18] T. Nishikawa, K. Goto, H. Murakami, Y. Kumagai, M. Uemukai, T. Tanikawa, and R. Katayama, "Observation of nanopipes in edge-defined film-fed grown β-Ga_2O_3 substrate and their effect on homoepitaxial surface hillocks," Jpn. J. Appl. Phys. **62**, SF1015 (2023).

[19] Y. Wang, G. N. Ali, M. K. Mikhov, V. Vaidyanathan, B. J. Skromme, B. Raghothamachar, and M. Dudley, "Correlation between morphological defects, electron beam-induced current imaging, and the electrical properties of 4H–SiC Schottky diodes," J. Appl. Phys. **97**, 013540 (2005).

[20] R. A. Berechman, M. Skowronski, S. Soloviev, and P. Sandvik, "Electrical characterization of 4H–SiC avalanche photodiodes containing threading edge and screw dislocations," J. Appl. Phys. **107**, 114504 (2010).

[21] S. Mu, M. Wang, H. Peelaers, and C. G. Van de Walle, "First-principles surface energies for monoclinic Ga_2O_3 and Al_2O_3 and consequences for cracking of $(Al_xGa_{1-x})_2O_3$," APL Mater. **8**, 091105 (2020).

[22] R. Schewski, M. Baldini, K. Irmscher, A. Fiedler, T. Markurt, B. Neuschulz, T. Remmele, T. Schulz, G. Wagner, Z. Galazka, and M. Albrecht, "Evolution of planar defects during homoepitaxial growth of β-Ga_2O_3 layers on (100) substrates—A quantitative model," J. Appl. Phys. **120**, 225308 (2016).

[23] A. Fiedler, R. Schewski, M. Baldini, Z. Galazka, G. Wagner, M. Albrecht, and K. Irmscher, "Influence of incoherent twin boundaries on the electrical properties of β-Ga_2O_3 layers homoepitaxially grown by metal-organic vapor phase epitaxy," J. Appl. Phys. **122**, 165701 (2017).

[24] R. Schewski, K. Lion, A. Fiedler, C. Wouters, A. Popp, S. V. Levchenko, T. Schulz, M. Schmidbauer, S. Bin Anooz, R. Grüneberg, Z. Galazka, G. Wagner, K. Irmscher, M. Scheffler, C. Draxl, and M. Albrecht, "Step-flow growth in homoepitaxy of β-Ga_2O_3 (100)—The influence of the miscut direction and faceting," APL Mater. **7**, 022515 (2019).

[25] S. Bin Anooz, R. Grüneberg, C. Wouters, R. Schewski, M. Albrecht, A. Fiedler, K. Irmscher, Z. Galazka, W. Miller, G. Wagner, J. Schwarzkopf, and A. Popp, "Step flow growth of β-Ga_2O_3 thin films on vicinal (100) β-Ga_2O_3 substrates grown by MOVPE," Appl. Phys. Lett. **116**, 182106 (2020).

[26] S. Roy, A. Bhattacharyya, P. Ranga, H. Splawn, J. Leach, and S. Krishnamoorthy, "High-k oxide field-plated vertical (001) β-Ga_2O_3 Schottky barrier diode with Baliga's figure of merit over 1 GW/cm^2," IEEE Electron Device Lett. **42**(8), 1140–1143 (2021).

[27] Z. Xia, H. Chandrasekar, W. Moore, C. Wang, A. J. Lee, J. McGlone, N. K. Kalarickal, A. Arehart, S. Ringel, F. Yang, and S. Rajan, "Metal/$BaTiO_3$/β-Ga_2O_3 dielectric heterojunction diode with 5.7 MV/cm breakdown field," Appl. Phys. Lett. **115**, 252104 (2019).

[28] J. B. Varley, A. Janotti, C. Franchini, and C. G. Van de Walle, "Role of self-trapping in luminescence and *p*-type conductivity of wide-band-gap oxides," Phys. Rev. B **85**, 081109 (2012).

[29] E. Farzana, A. Bhattacharyya, N. S. Hendricks, T. Itoh, S. Krishnamoorthy, and J. S. Speck, "Oxidized metal Schottky contact with high-*K* dielectric field plate for low-loss high-power vertical β-Ga_2O_3 Schottky diodes," APL Mater. **10**, 111104 (2022).

[30] Z. Han, G. Jian, X. Zhou, Q. He, W. Hao, J. Liu, B. Li, H. Huang, Q. Li, X. Zhao, G. Xu, and S. Long, "2.7 kV low leakage vertical PtO_x/β-Ga_2O_3 Schottky barrier diodes with self-aligned mesa termination," IEEE Electron Device Lett. **44**(10), 1680–1683 (2023).

[31] B. Cromer, D. Saraswat, N. Pieczulewski, W. Li, K. Nomoto, F. V. E. Hensling, K. Azizie, H. P. Nair, D. G. Schlom, D. A. Muller, D. Jena, and H. G. Xing, "Over 6 MV/cm operation in β-Ga_2O_3 Schottky barrier diodes with IrO_2 and RuO_2 anodes deposited by molecular beam epitaxy," J. Vac. Sci. Technol., A. **42**(3), 033206 (2024).

[32] F. V. E. Hensling, C. T. Parzyck, B. Cromer, M. A. Al Mamun, Y. E. Suyolcu, L. Kalaydjian, I. Subedi, J. Park, K. Azizie, Q. Song, P. A. van Aken, N. J. Podraza, K. Cho, D. Jena, H. G. Xing, K. M. Shen, D. G. Schlom, and P. Vogt, "Growth of tetragonal PtO by molecular-beam epitaxy and its integration into β-Ga_2O_3 Schottky diodes," APL Mater. **13**, 111108 (2025).

[33] Z. Li, M. Grimsditch, C. M. Foster, and S.-K. Chan, "Dielectric and elastic properties of ferroelectric materials at elevated temperature," J. Phys. Chem. Solids **57**(10), 1433–1438 (1996).

[34] J. Rehm, T.-S. Chou, S. B. Anooz, P. Seyidov, A. Fiedler, Z. Galazka, and A. Popp, "Perspectives on MOCVD-grown (100) β-Ga_2O_3 thin films and its Al-alloy for power electronics application," Appl. Phys. Lett. **121**, 240503 (2022).

[35] D. J. Harra and T. W. Snouse, "A radiant heated titanium sublimator," J. Vac. Sci. Technol. **9**, 552–555 (1972).

[36] C. D. Theis and D. G. Schlom, "Cheap and stable titanium source for use in oxide molecular beam epitaxy systems," J. Vac. Sci. Technol., A. **14**, 2677–2679 (1996).

[37] G. Koster, B. L. Kropman, G. J. H. M. Rijnders, D. H. A. Blank, and H. Rogalla, "Quasi-ideal strontium titanate crystal surfaces through formation of strontium hydroxide," Appl. Phys. Lett. **73**, 2920–2922 (1998).

[38] N. A. Parker, P. Buragohain, S. Lee, K. Azizie, A. Oni, G. N. Kotsonis, A. Ross, L.-Q. Chen, P. Debashis, R. Kim, R. Steinhardt, and D. G. Schlom, "Impact of non-stoichiometry on the spontaneous polarization and coercive field of ferroelectric $BaTiO_3$ grown by molecular-beam epitaxy" (unpublished).

[39] P. Vogt, F. V. E. Hensling, K. Azizie, C. S. Chang, D. Turner, J. Park, J. P. McCandless, H. Paik, B. J. Bocklund, G. Hoffman, O. Bierwagen, D. Jena, H. G. Xing, S. Mou, D. A. Muller, S.-L. Shang, Z.-K. Liu, and D. G. Schlom, "Adsorption-controlled growth of Ga_2O_3 by suboxide molecular-beam epitaxy," APL Mater. **9**, 031101 (2021).

[40] K. Azizie, F. V. E. Hensling, C. A. Gorsak, Y. Kim, N. A. Pieczulewski, D. M. Dryden, M. K. I. Senevirathna, S. Coye, S.-L. Shang, J. Steele, P. Vogt, N. A. Parker, Y. A. Birkhölzer, J. P. McCandless, D. Jena, H. G. Xing, Z.-K. Liu, M. D. Williams, A. J. Green, K. Chabak, D. A. Muller, A. T. Neal, S. Mou, M. O. Thompson, H. P. Nair, and D. G. Schlom, "Silicon-doped β-Ga_2O_3 films grown at 1 μm/h by suboxide molecular-beam epitaxy," APL Mater. **11**, 041102 (2023).

[41] D. Wang, L. He, Y. Le, X. Feng, C. Luan, H. Xiao, and J. Ma, "Characterization of single crystal β-Ga_2O_3 films grown on $SrTiO_3$ (100) substrates by MOCVD," Ceram. Int. **46**, 4568–4572 (2020).

[42] J. Åhman, G. Svensson, and J. Albertsson, "A reinvestigation of β-gallium oxide," Acta Crystallogr., Sect. C:Cryst. Struct. Commun. **52**(6), 1336–1338 (1996).

[43] T. Nakatani, A. Yoshiasa, A. Nakatsuka, T. Hiratoko, T. Mashimo, M. Okube, and S. Sasaki, "Variable-temperature single-crystal X-ray diffraction study of tetragonal and cubic perovskite-type barium titanate phases," Acta Crystallogr., Sect. B: Struct. Sci., Cryst. Eng. Mater. **72**(1), 151–159 (2016).

[44] R. W. Balluffi, A. Brokman, and A. H. King, "CSL/DSC Lattice model for general crystalcrystal boundaries and their line defects," Acta Metall. **30**(8), 1453–1470 (1982).

[45] W. Friedrich, P. Knipping, and M. Laue, "Interferenzerscheinungen bei röntgenstrahlen," Ann. Phys. **346**(10), 971–988 (1913).

[46] H. Kiessig, "Interferenz von röntgenstrahlen an dünnen schichten," Ann. Phys. **402**(7), 769–788 (1931).

[47] Y. Matsubara, K. S. Takahashi, Y. Tokura, and M. Kawasaki, "Single-crystalline $BaTiO_3$ films grown by gas-source molecular beam epitaxy," Appl. Phys. Express **7**(12), 125502 (2014).

[48] W. Nunn, S. Sandlass, M. Wegner, R. Haislmaier, A. Kumar, M. Tangi, J. LeBeau, E. Quandt, R. D. James, and B. Jalan, "Hybrid molecular beam epitaxy growth of $BaTiO_3$ films," J. Vac. Sci. Technol., A. **39**, 040404 (2021).

[49] B. Fazlioglu-Yalcin, A. C. Suceava, T. Kuznetsova, K. Wang, V. Gopalan, and R. Engel-Herbert, "Stoichiometric control and optical properties of $BaTiO_3$ thin films grown by hybrid MBE," Adv. Mater. Interfaces **10**(11), 2300018 (2023).

[50] P. Abbasi, N. Shirato, R. E. Kumar, I. V. Albelo, M. R. Barone, D. N. Cakan, M. d. l. P. Cruz-Jáuregui, S. Wieghold, D. G. Schlom, V. Rose, T. A. Pascal, and D. P. Fenning, "Nanoscale surface structure of nanometer-thick ferroelectric $BaTiO_3$ films revealed by synchrotron X-ray scanning tunneling microscopy: Implications for catalytic adsorption reactions," ACS Appl. Nano Mater. **6**(3), 2162–2170 (2023).

[51] J. B. Nelson and D. P. Riley, "An experimental investigation of extrapolation methods in the derivation of accurate unit-cell dimensions of crystals," Proc. Phys. Soc. London **57**, 160–177 (1945).

[52] S. Mu, H. Peelaers, Y. Zhang, M. Wang, and C. G. Van de Walle, "Orientation-dependent band offsets between $(Al_xGa_{1-x})_2O_3$ and Ga_2O_3," Appl. Phys. Lett. **117**, 252104 (2020).

[53] T.-S. Chou, P. Seyidov, S. B. Anooz, R. Grüneberg, M. Pietsch, J. Rehm, T. T. V. Tran, K. Tetzner, Z. Galazka, M. Albrecht, K. Irmscher, A. Fiedler, and A. Popp, "Suppression of particle formation by gas-phase pre-reactions in (100) MOVPE-grown β-Ga_2O_3 films for vertical device application," Appl. Phys. Lett. **122**, 052102 (2023).

Supplementary Material

Growth of *a*-plane $BaTiO_3$ on *a*-plane β-Ga_2O_3 by Molecular-Beam Epitaxy

Kathy Azizie,[1] Naomi A. Pieczulewski,[1] Nicholas A. Parker,[1] Jian V. Li,[2,3] Nolan S. Hendricks,[4] Kyle J. Liddy,[4] Yorick A. Birkhölzer,[1] Eric A. Welp,[5] Luke Omodt,[5] Thaddeus J. Asel,[2] Shin Mou,[2] David A. Muller,[6,7] and Darrell G. Schlom[1,6,8,a]

[1]Department of Materials Science and Engineering, Cornell University, Ithaca, New York 14853, USA
[2]Air Force Research Laboratory, Materials and Manufacturing Directorate, Wright Patterson Air Force Base, Ohio 45433, USA
[3]Core4ce, Beavercreek, Ohio 45324, USA
[4]Air Force Research Laboratory, Sensors Directorate, Wright Patterson Air Force Base, Ohio 45433, USA
[5]Platform for the Accelerated Realization, Analysis, and Discovery of Interface Materials, Cornell University, Ithaca, New York 14853, USA
[6]Kavli Institute at Cornell for Nanoscale Science, Ithaca, New York 14853, USA
[7]School of Applied and Engineering Physics, Cornell University, Ithaca, New York 14853, USA
[8]Leibniz-Institut für Kristallzüchtung, Max-Born-Str. 2, 12489 Berlin, Germany

[a]Author to whom correspondence should be addressed: schlom@cornell.edu

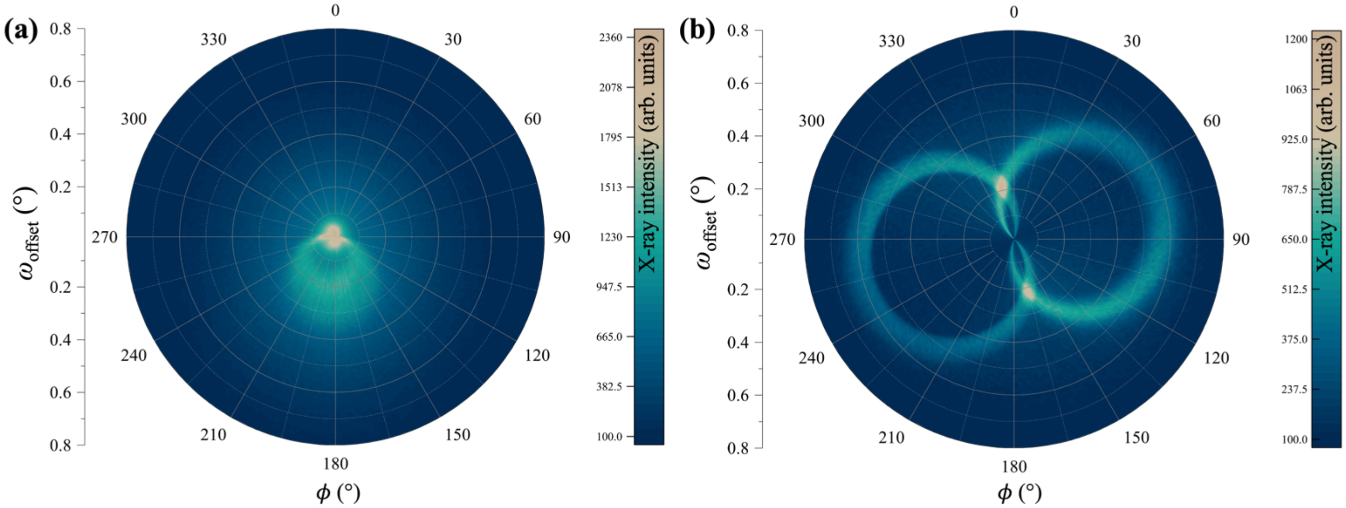

Figure S1: Pole figures about the 100 $BaTiO_3$ film peak of (a) sample C and (b) sample B. Pole figure (a) was generated by stitching ϕ scans over a suitable ω range that encompasses the peak of interest. Pole figure (b) was generated by collecting ω scans of the film peak about the entire range of ϕ.

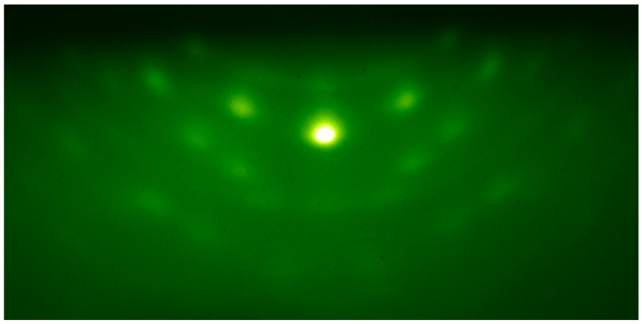

Figure S2: RHEED pattern of a $BaTiO_3$ film grown on (100) β-Ga_2O_3 at T_{sub} = 560 °C. At this low temperature the film is observed to be polycrystalline.

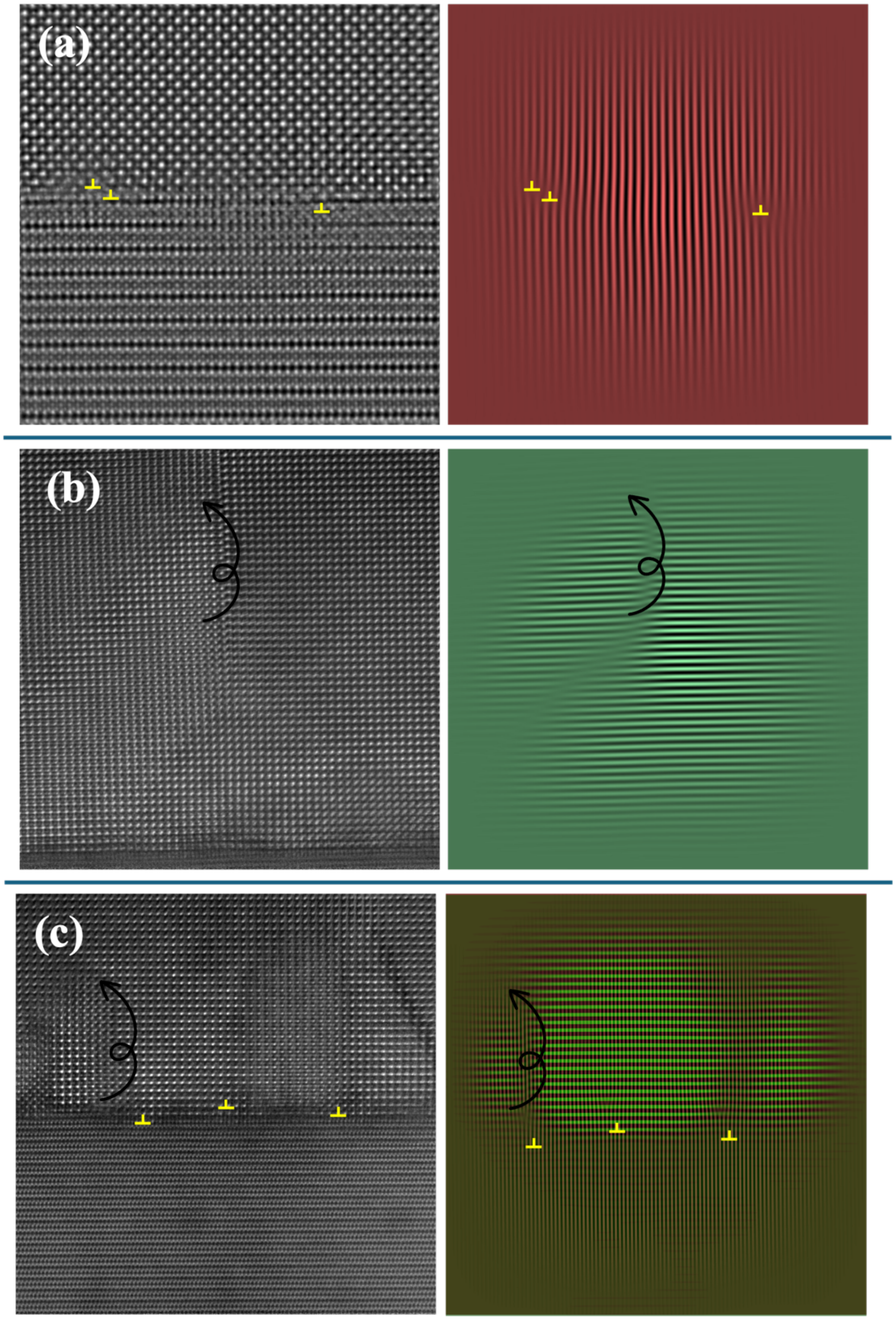

Figure S3: Atomic-resolution HAADF-STEM images of three separate regions of the $BaTiO_3/Ga_2O_3$ interface of sample C with corresponding in-plane diffraction peak masking to identify edge and screw dislocations as shown.

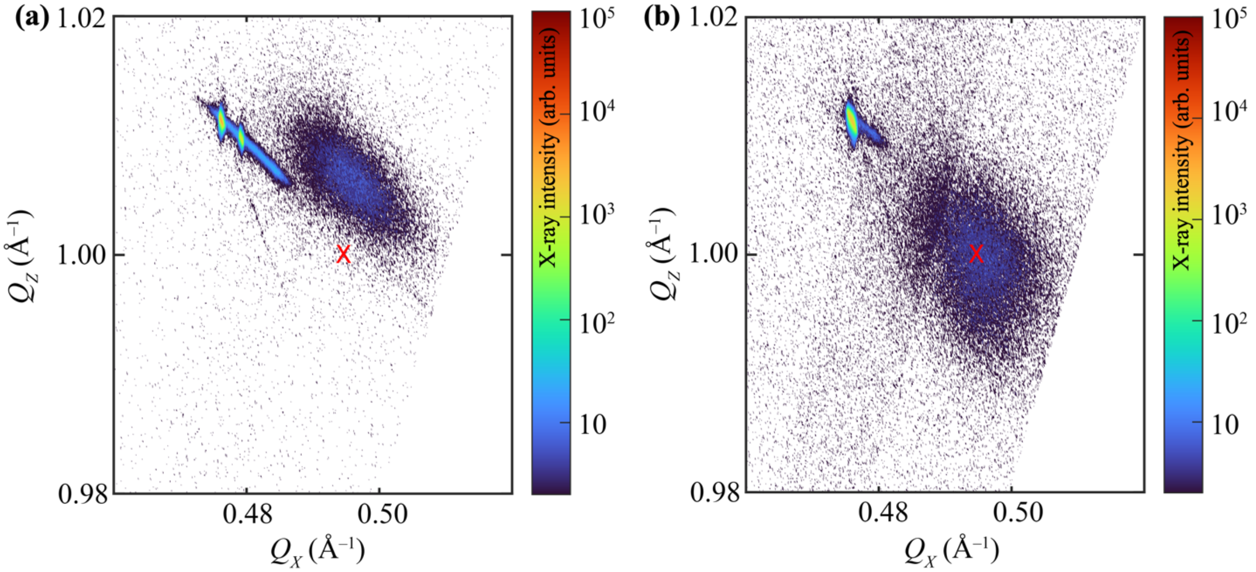

Figure S4: Reciprocal space maps (RSMs) showcasing both the 402 $BaTiO_3$ peak (the broad blue peak) and the $\underline{11}12$ *a*-plane oriented Ga_2O_3 peak(s) of (a) sample C and (b) sample G, where Q_Z is out-of-plane and Q_X is in-plane. Overlaid on both as a red X is the expected position of the 402 peak of bulk (relaxed) $BaTiO_3$ (with lattice constants $a = 3.998$ Å and $c = 4.035$ Å). Both figures show in-plane relaxation to the bulk value of $BaTiO_3$ while sample C shows out-of-plane strain based off its displacement in Q_Z. This difference in strain could be due to stoichiometry differences between these two samples; sample G is closer to being stoichiometric as seen in the XRD scans of sample C and G (Figs. 2 and 5, respectively).

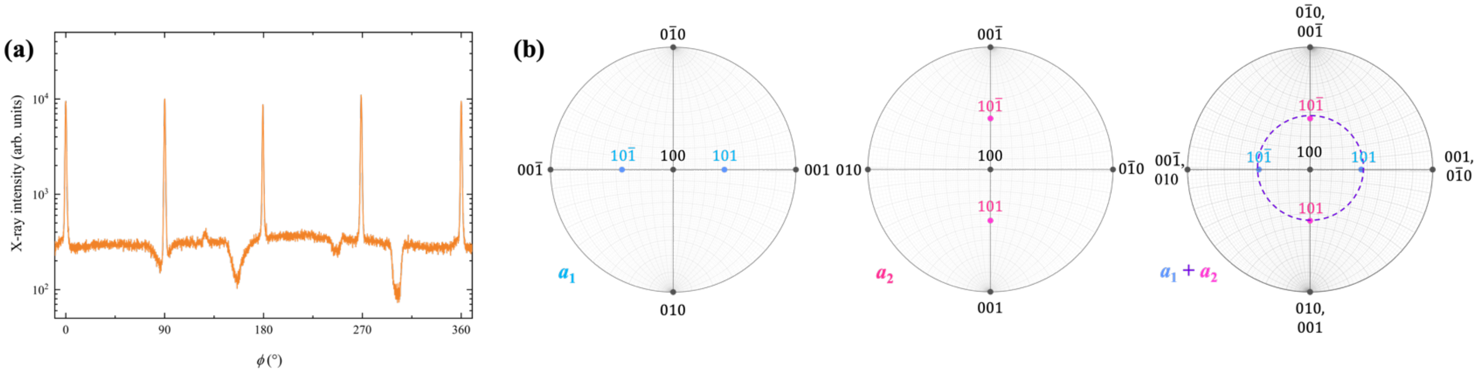

Figure S5: (a) Shows a ϕ scan of the {101} family of $BaTiO_3$ peaks (with $2\theta = 31.48°$ and $\chi \approx 45$) of sample C with $\phi = 0°$ being aligned to be parallel to the [001] in-plane projection of the (100) $BaTiO_3$ film. (b) showcases a series of stereographic projections of *a*-plane oriented $BaTiO_3$ with the {101} family of $BaTiO_3$ peaks shown for an a_1 domain (blue), a_2 domain (pink), and a mixture of a_1 and a_2 domains. The emergence of four distinct peaks at 90° intervals instead of two is consistent with a mixture of a_1 and a_2 domains rather than one domain type being dominant.

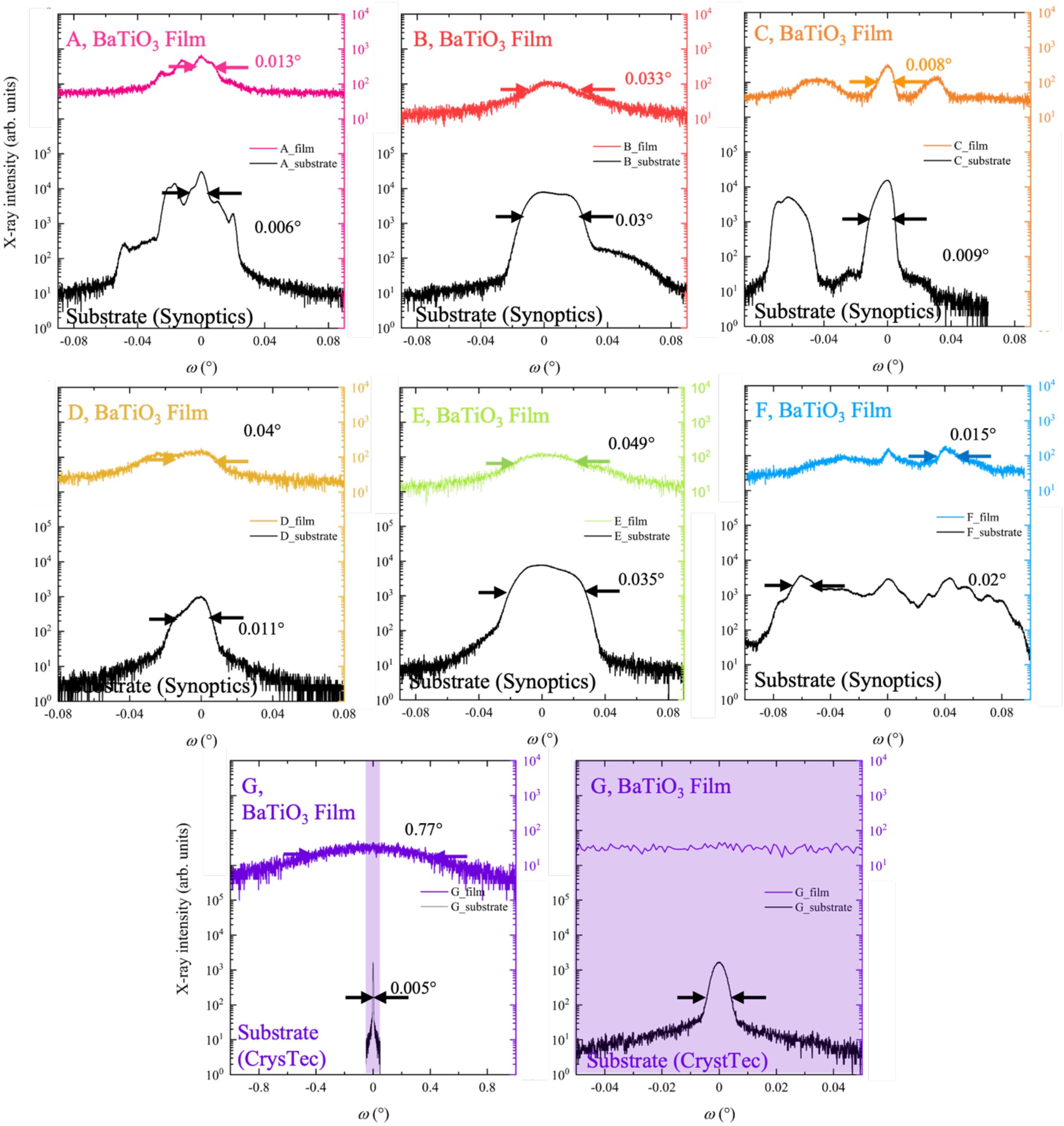

Figure S6: Rocking curves of all films listed in Table I overlaid on the rocking curves of each corresponding substrate. The FWHM of each film and substrate peak is given and indicated by arrows. Sample G is plotted twice because the FWHM of the film is more than 100× broader than that of the substrate.

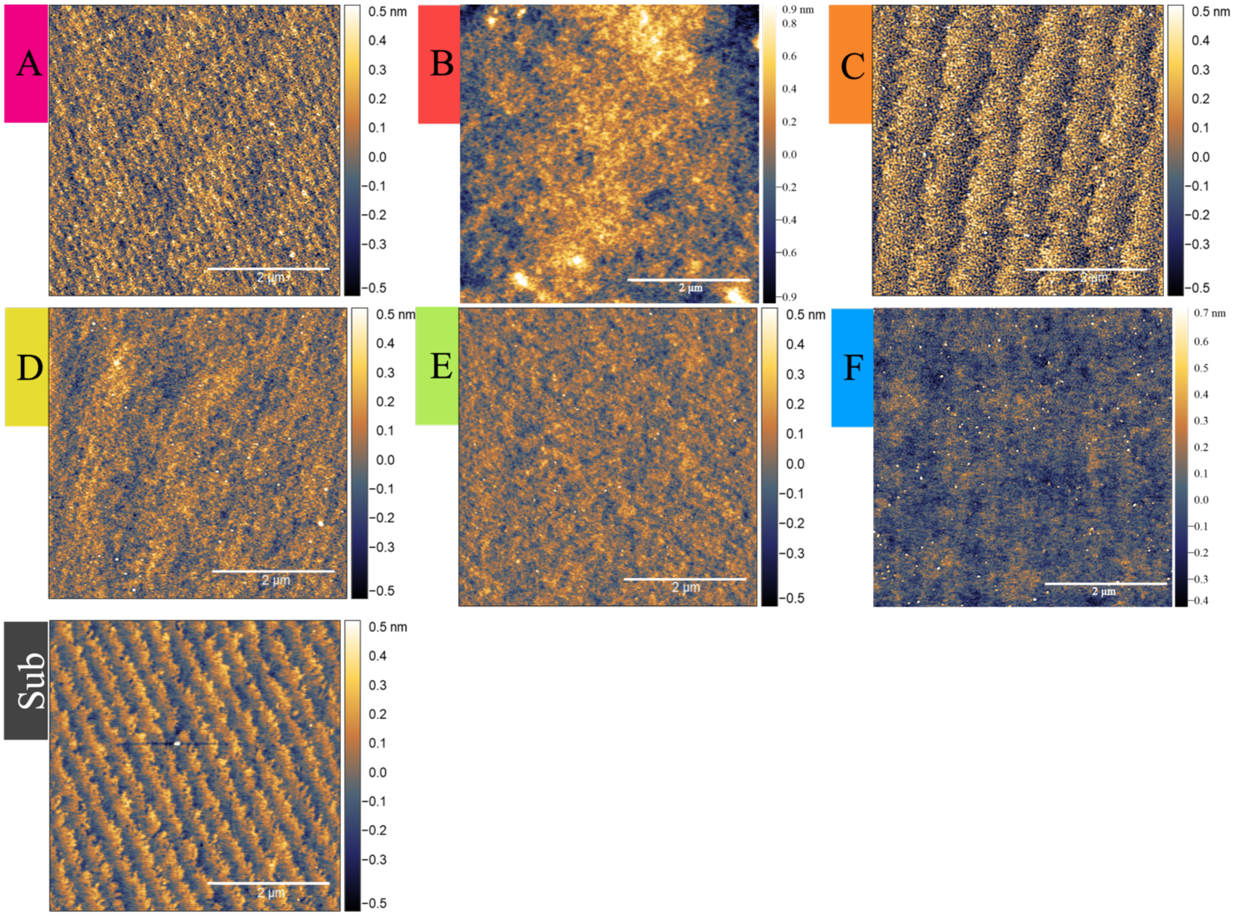

Figure S7: AFM scans of all films listed in Table I and of a bare (100) Ga_2O_3 substrate out of the box (boule material provided by Synoptics and oriented, cut, and polished by CrysTec).